https://doi.org/10.3311/PPee.43122

Periodica Polytechnica Electrical Engineering and Computer Science

New Combined MTPA–VCLMT–CPR Control Strategy for IPMSM Drives in Vehicle Propulsion System

Norediene Aouadj[1*], Kada Hartani[2], Abdelkader Merah[2], Yassine Boudouaoui[1]

[1] Second Cycle Department, Higher School of Electrical and Energetic Engineering (ESGEEO), Chemin Vicinal 9., 31000 Oran, Algeria
[2] Electrotechnical Engineering Laboratory, Electrotechnical Department, Faculty of Technology, University of Saida Dr. Moulay Tahar, 20000 Ennasr, Saida, P.O.B. 138, Algeria
[*] Corresponding author, e-mail: aouadj.norediene@esgee-oran.dz

Received: 18 December 2025, Accepted: 05 May 2026, Published online: 14 May 2026

Abstract

The control of electric vehicles (EVs) is achieved through the management of their in-wheel motors, which are part of the electric traction system. This study has derived an algorithm strategy for the operation of interior permanent magnet synchronous motors (IPMSM) used in high-speed electric traction applications. The strategy combines the maximum torque per ampere control (MTPA) for low speeds and the control of the Voltage Current Limited Maximum Torque (VCLMT) and the Constant Power Region (CPR) for high speeds. By implementing this strategy, precise and independent control of the torque applied to each in-wheel motor is achieved, ensuring high torque at high speeds. This level of control is crucial for embedded systems. IPMSMs have been identified as a promising choice for electric vehicle applications due to their ability to generate reluctance torque, as well as their higher efficiencies, torque, and power densities. To ensure the smooth functioning of the IPMSM motor, a crucial component in electric vehicles, the proposed method incorporates a combination of three torque control strategies and divides the torque/speed characteristics into five distinct zones. The effectiveness of this strategy was confirmed through extensive simulation using MATLAB/Simulink. The numerical simulation results demonstrate exceptional traction system dynamics across a wide range of operating speeds.

Keywords

MTPA, VCLMT, CPR, IPMSM, electric vehicle, in-wheel motor

1 Introduction

Electric vehicles have been emphasized as a practical and effective way to address both energy issues and environmental concerns. Additionally, EVs offer numerous benefits in comparison to traditional internal combustion engine vehicles due to the utilization of electric motors and inverters in their drivetrains [1]. Electric vehicles possess superior control capabilities in comparison to internal combustion engine vehicles (ICEVs), allowing them to not only provide a clean mode of transportation but also achieve enhanced levels of safety and handling [2, 3].

Unlike motors used in industrial applications, the traction motors utilized in electric vehicles must be capable of frequent starts and stops, rapid acceleration and deceleration, high torque for hill climbing at low speeds, and low torque for cruising at high speeds. Additionally, these traction motors must exhibit two crucial characteristics: a fast and robust torque response that can cater to the driver's instantaneous torque requirements across a wide range of speeds, and a minimal torque ripple that does not exceed ±2% to prevent uncomfortable mechanical vibrations and vehicle noise [4].

The management of an electric vehicle relies on the regulation of its traction chain, specifically through the control of the in-wheel motors. In the realm of industrial motor drive applications, the direct torque control (DTC) scheme for PMSM drives has garnered significant attention due to its potential benefits and practicality in embedded systems, particularly in the context of electric vehicles. However, a major drawback of direct torque control is the occurrence of high torque ripple, which can be attributed to the presence of hysteresis controllers and the limited number of available voltage vectors [4].

In response to this issue, various approaches have recently emerged with the aim of achieving rapid and

Cite this article as: Aouadj, N., Hartani, K., Merah, A., Boudouaoui, Y. "New Combined MTPA–VCLMT–CPR Control Strategy for IPMSM Drives in Vehicle Propulsion System", Periodica Polytechnica Electrical Engineering and Computer Science, 2026. https://doi.org/10.3311/PPee.43122

robust torque response, while also addressing the negative impact of torque ripple on the mechanical transmission of the electric traction chain [5–8]. In Aouadj et al. [4], the authors present a novel approach to enhancing the dynamic capabilities of direct torque control (DTC) and reducing torque fluctuations in PMS in-wheel electric motors used for vehicle propulsion. They introduce a new sliding mode backstepping control technique as a means to achieve these objectives. Additionally, the study includes the design of a sliding mode controller with an exponential reaching law, as detailed in reference [4].

Interior permanent magnet synchronous motors (IPMSM) have emerged as a promising choice for electric vehicle (EV) applications within the realm of AC electric motors. Their notable advantages, such as a higher mass torque when compared to conventional asynchronous motors, make them ideal for embedded applications [5, 6]. These motors are renowned for their efficiency, as well as their lightweight and compact design [7]. In IPMSM motors, the quadrature inductance surpasses the direct inductance, resulting in a torque that combines the excitation torque of the magnet and the reluctance torque, which is a significant advantage. Additionally, the IPMSM capitalizes on the nonlinear term present in the expression of its electromagnetic torque [8, 9]. Furthermore, IPMSM drives are well-suited for flux-weakening, enabling constant power operation across a wide range of speeds [10].

Four-wheel independent drive (4WID), also known as in-wheel motor, has become a common configuration in electric vehicles. These in-wheel motors are responsible for controlling the vehicle's movement. The performance of the wheel-motor system is characterized by smooth rotation across all motor speeds, torque control at zero speed, and quick acceleration and deceleration. To meet the demand for fast and reliable torque response in a wide speed range, various controls for in-wheel electrical motors have been developed. One widely used control method is Field Oriented Control (FOC), which was first proposed by both Hasse and Blaschke around 1968–1971 and is commonly applied to AC motor control. In recent years, the direct FOC (DFOC) for IPMSM drives has gained significant attention in EV-traction due to its ability to operate at high speeds and a wider speed range through flux weakening control [11]. In Liu et al. [12], a presentation is made on the implementation of Vector Control Technology for Permanent Magnet Synchronous Motors (PMSM) in Electric Vehicles, utilizing the space vector pulse width modulation (SVPWM) algorithm.

In this paper, we present a novel approach to controlling IPMSM in a wide range of speeds. Our work focuses on developing a new control strategy that combines maximum torque per ampere control (MTPA) at low speeds and voltage current limited maximum torque (VCLMT) and constant power region (CPR) at high speeds. This strategy, based on vector control (FOC), is specifically designed for electric vehicles equipped with four IPMS in-wheel motors during traction or regenerative braking modes. By combining three torque control strategies and dividing the torque/speed characteristics into five zones, our proposed approach ensures optimal operation for the IPMSM machine across a wide speed range. To achieve high torque at high speeds, the motor needs to be defluxed by introducing a negative current along the *d*-axis [13]. We will describe various methods for generating reference currents based on the operating speed, reference torque, and voltage and current constraints [14].

To reduce the amplitude of the back-electromotive voltage without slowing down the machine's rotation, a current can be injected on the ***d***-axis. This axis aligns with the flux of the permanent magnets, so injecting a current in the same direction that amplifies the magnet's flux. Conversely, injecting a current in the opposite direction partially cancels out the permanent magnet's flux, resulting in a flux weakening. This flux weakening reduces the back-electromotive voltage, enabling a higher current to be injected on the torque axis and generating more torque at high speeds. Referred to as flux weakening (FW) control, this method offers the benefit of enabling the machine to operate at higher angular speeds, a crucial factor for electric vehicles. In the context of permanent magnet motors used in vehicle traction, there is a well-known issue of needing to reduce the magnetic flux at elevated speeds [15]. To address this, the technique of flux weakening in an interior permanent magnet synchronous motor (IPMSM) involves introducing a demagnetizing current along the d-axis. Another approach, proposed in Barbini et al. [15], suggests utilizing centrifugal force to significantly decrease the magnetic flux of the permanent magnet.

To ensure optimal performance of IPMSM-drives in electric vehicles, the utilization of MTPA control is crucial for its high torque output. Additionally, FW control is necessary to generate increased torque in the high-speed range [16, 17]. This study investigates the torque–speed characteristics of the machine, which are divided into five operating regions governed by three control strategies: Maximum Torque per Ampere (MTPA), Voltage–Current

Limited Maximum Torque (VCLMT), and Constant Power Region (CPR) control. In the low-speed region (below base speed), the electromagnetic torque is limited by the maximum torque condition defined by the MTPA strategy. When the operating speed exceeds the base speed, the torque gradually decreases while the motor maintains maximum constant power [18].

To extend the operating range, a flux-weakening technique is employed [19]. However, depending on the machine parameters, field-weakening control may lead to suboptimal torque distribution, resulting in reduced torque capability. Consequently, the machine operates within the power-limited region, namely the constant power region (CPR) [20].

To enhance driving efficiency and ensure stable operation under high-speed and high-torque conditions in electric vehicle applications, this work proposes a vector control strategy for an Interior Permanent Magnet Synchronous Motor (IPMSM) in-wheel drive. The proposed method integrates MTPA, VCLMT, and CPR control strategies to optimize motor performance across the entire operating range.

2 Conception of combined MTPA-VCLMT-CPR control of IPMSM

To ensure optimal torque performance across a wide range of speeds, a decision was made to combine and utilize two distinct control strategies. At low speeds within the constant torque region, a MTPA control is employed, as depicted in Fig. 1. This control strategy maintains a constant current on the axes, ensuring a consistent torque output until the base speed is reached. Conversely, in the constant power region where the developed torque gradually decreases, a FW control is implemented. This control strategy enables the motor to generate high output torque in the high-speed region without surpassing the rated current. It is worth noting that this algorithm also facilitates the operation of the IPMSM at higher speeds, expanding its speed range [17, 21].

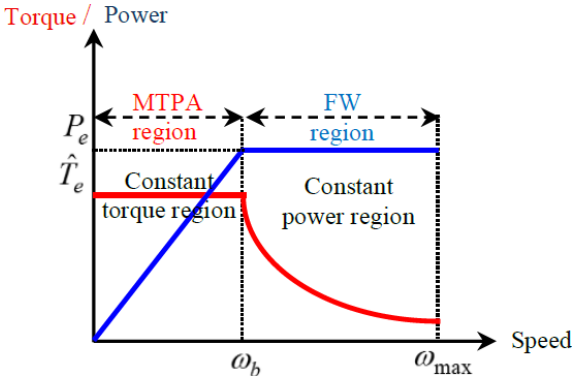

Fig. 1 Typical characteristic curves of torque/power *vs*. speed of IPMSMs

2.1 Mathematical model of IPMSM

Upon applying Park's transformation and adjusting the reference frame *dq*, the stator equations of the IPMSM with respect to the rotor can be expressed as follows:

The voltage equations are provided as:

$$v_d = R_s i_d + L_d \frac{di_d}{dt} - \omega_e L_q i_q, \tag{1}$$

$$v_q = R_s i_q + L_q \frac{di_q}{dt} + \omega_e \left(\Phi_f + L_d i_d\right), \tag{2}$$

whrere R_s is the stator winding resistance, L_d is the *d*-axis inductance, L_q is the ***q***-axis inductance, i_d the ***d***-axis current, i_q is the *q*-axis current and Φ_f is the permanent magnet flux.

The expression for the developed motor torque can be represented as follows:

$$T_e = \frac{3}{2} p\Phi_f i_q + \frac{3}{2} p\left(L_d - L_q\right) i_d i_q, \tag{3}$$

The mechanical torque involves determining its value.

$$T_e - T_L - f\omega_m = J\frac{d\omega_m}{dt}. \tag{4}$$

where ω_e is the rotor electrical speed, ω_m is rotor mechanical speed, T_{load} is the load torque, $T_{\text{friction}} = f\omega_m$ is the motor-load system friction torque, f viscous coefficient of friction, and $J = J_m + J_\omega$ is the moment of inertia of the motor and the wheel.

2.2 MTPA control technique

To achieve optimal torque output based on a specific current, the currents in the ***d***- and ***q***-axes can be expressed as [22, 23]:

$$i_d = \hat{I}_s \cos\beta, \tag{5}$$

$$i_q = \hat{I}_s \sin\beta. \tag{6}$$

In Fig. 2 [22], the "torque angle" $\beta\left(180° \succ \beta \geq 0°\right)$ is defined as the angle between the stator phase current vector and the negative direction of the ***d***-axis, while $\hat{I}_s$ represents the magnitude of the stator phase current in an IPM motor.

The developed torque in IPMSM motors can be viewed as a combination of the magnet's excitation torque T_{mag} and the reluctant torque T_{rel}, as shown in Fig. 3. This is because the ***q***-axis reactance/inductance is larger than the ***d***-axis

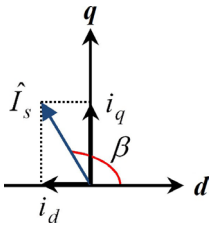

Fig. 2 Torque angle

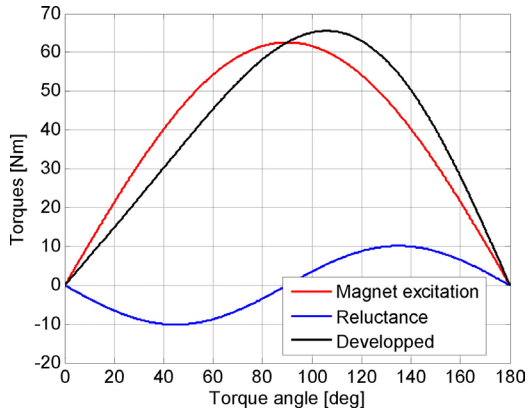

Fig. 3 Developed torque, magnet excitation torque and reluctance torque *vs*. torque angle of IPMSM

reactance/inductance, resulting i.e., $L_q > L_d$. The expression for the developed torque is as follows [23]:

$$T_e = T_{mag} + T_{rel}, \tag{7}$$

where:

$$T_{mag} = \frac{3}{2} p\Phi_f \hat{I}_s \sin\beta, \tag{8}$$

$$T_{rel} = \frac{3}{2} p\left(L_d - L_q\right)\hat{I}_s^2 \frac{\sin 2\beta}{2}. \tag{9}$$

In the constant torque region of an on-board interior permanent magnet synchronous motor (IPMSM), there exists a specific combination of ***d***- and ***q***-axis currents that maximizes torque output. This algorithm, known as maximum torque per ampere (MTPA), is utilized to meet the high torque demands of traction applications like electric vehicles (EVs). The ***q***-axis current can be mathematically represented as shown in Eq. (10) [17].

$$i_q = \sqrt{i_s^2 - i_d^2} \tag{10}$$

The torque angle which results in the maximum torque of IPMSM motors can be derived by setting the derivative of the torque to zero, which can be expressed as follows:

$$\frac{dT_{em}}{d\beta} = \frac{3}{2} p\left(\Phi_f \hat{I}_s \cos\beta + \left(L_d - L_q\right)\hat{I}_s^2 \cos 2\beta\right) = 0. \tag{11}$$

The ***d***-axis current during MTPA operation is obtained as follows:

$$i_{d_{\text{MTPA}}} = \frac{\Phi_f}{4\left(L_d - L_q\right)} - \sqrt{\frac{\Phi_f^2}{16\left(L_d - L_q\right)^2} + \frac{\hat{I}_s^2}{2}}. \tag{12}$$

By substituting Eq. (12) into Eq. (10), it is possible to derive the ***q***-axis current in MTPA operation with simplicity.

$$i_{q_{\text{MTPA}}} = \sqrt{\hat{I}_s^2 - i_{d_{\text{MTPA}}}^2} \tag{13}$$

When the current falls below I_{sn}, the operating point on the MTPA curve shifts downwards. Once the motor reaches the base speed ω_b, which is determined by the intersection of the current limit circle and the voltage limit ellipse, it has reached its maximum current and voltage [24].

We will then give:

$$\omega_b = \frac{V_{sn}}{p\sqrt{\left(\Phi_f + L_d i_{d_{\max}}\right)^2 + \left(L_q i_{q_{\max}}\right)^2}}. \tag{14}$$

2.3 VCLMT control

If the operation goes beyond the base speed ω_b, the Voltage and Current Limited Maximum Torque (VCLMT) control strategy can deliver a higher torque compared with MTPA control. The operating locus of VCLMT is determined by the intersection between the maximum current limit circle and the voltage limit ellipse at a specific speed ω_r, which defines the new VCLMT operating locus $\left(i_{d_{\text{VCLMT}}}, i_{q_{\text{VCLMT}}}\right)$ in the plane (i_d, i_q). his intersection forms the trajectory for the VCLMT command [24].

$$i_{d_{\text{VCLMT}}} = \frac{-\Phi_f L_d}{L_d^2 - L_q^2} + \frac{\sqrt{\left(\Phi_f L_d\right)^2 - \left(L_d^2 - L_q^2\right)\left(\Phi_f^2 + L_q^2 \hat{I}_{\max}^2 - \left(\frac{V_{\max}}{p\omega_r}\right)^2\right)}}{L_d^2 - L_q^2} \tag{15}$$

$$i_{q_{\text{VCLMT}}} = \sqrt{\hat{I}_{\max}^2 - i_{d_{\text{VCLMT}}}^2} \tag{16}$$

2.4 Constant Power Region control

According to the Constant Power Region (CPR) [24], torque is defined as follows:

$$P = C_{em}\omega_r = \frac{3}{2}\left(\Phi_f i_q + \left(L_d - L_q\right) i_d i_q\right)\omega_r. \tag{17}$$

The power output of the IPMSM is represented by the variable *P*. The trajectory that represents this power

can be determined by solving a fourth-order equation, as stated in Itani [24].

$$\begin{aligned}&\left(L_d-L_q\right)^2 i_d^4+2\Phi_f\left(L_d-L_q\right)i_d^3\\&+\left(\Phi_f^2-\left(L_d-L_q\right)^2\hat{I}_{\max}^2\right)i_d^2\\&-2\Phi_f\left(L_d-L_q\right)\hat{I}_{\max}^2 i_d+\frac{4\cdot P^2}{9\cdot\omega_e^2}-\Phi_f^2\hat{I}_{\max}^2=0\end{aligned}\tag{18}$$

To achieve the desired outcome, it is imperative to select a solution for $i_{d_{\mathrm{CPR}}}$ that is both negative in value and in close proximity to zero. By doing so, we can successfully derive the corresponding value for $i_{q_{\mathrm{CPR}}}$.

$$i_{q_{\mathrm{CPR}}}=\sqrt{\hat{I}_{\max}^2-i_{d_{\mathrm{CPR}}}^2}\tag{19}$$

At a specific speed ω_{inter}, the torque produced by CPR control exceeds that generated by VCLMT control. Once this speed is reached, the control strategy shifts to CPR to achieve higher torque while maintaining constant power.

3 Combination of three control strategies

By integrating three MTPA/VCLMT/CPR control strategies, the maximum torque in relation to motor operating speed was successfully achieved, as demonstrated in Fig. 4 for torque/speed and Fig. 5 for power/speed [24].

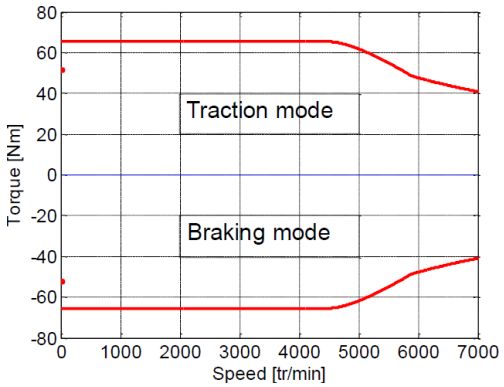

Fig. 4 Torque/speed characteristics with combined control strategy

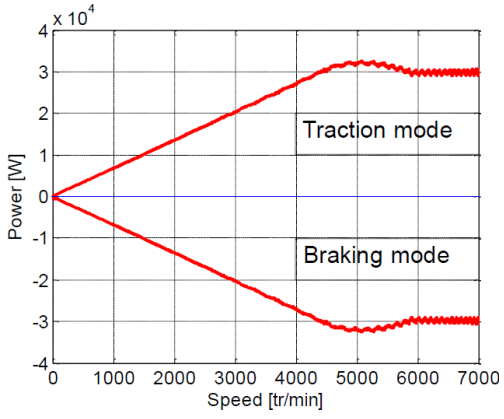

Fig. 5 Power/speed characteristics with combined control strategy

T_{em} is the defined maximum torque attained through the three control methods: MTPA, VCLMT, and CPR. In the case that the reference torque exceeds the maximum torque available at a specific speed ω_r, the reference torque is adjusted accordingly.

$$\begin{cases}0\le\omega_r<\omega_b\Rightarrow T_{em}^*\Rightarrow T_{em_{\max\mathrm{MTPA}}}^*\\ \omega_b\le\omega_r<\omega_{\mathrm{inter}}\Rightarrow T_{em}^*=T_{em_{\max\mathrm{VCLMT}}}^*\\ \omega_r\ge\omega_{\mathrm{inter}}\Rightarrow T_{em}^*=T_{em_{\max\mathrm{CPR}}}^*\end{cases}\tag{20}$$

Fig. 6 shows the division of the control domain into five distinct zones. The initial zone is specifically designated for speeds below the base speed ω_b. Within this particular region, the MTPA control strategy imposes limitations on the maximum attainable torque. It is imperative that our system has the capability to deliver a torque value that falls below $T_{em_{\max\mathrm{MTPA}}}^*$.

Between speeds ω_b and $\omega_{end_{\mathrm{MTPA}}}$, the MTPA trajectory creates a boundary for the zone below $T_{em_{\max}}^*$, resulting in the formation of two separate areas: Zone II and Zone III. The region between $\omega_{end_{\mathrm{MTPA}}}$ and ω_{inter} is designated as Zone IV.

At higher speeds than ω_{inter} in Zone V, it is possible to achieve a lower torque amplitude compared to $T_{em_{\max\mathrm{VCLMT}}}^*$. However, for higher torques, the only option is the torque specified by $T_{em_{\max\mathrm{CPR}}}^*$ [24].

The generation of reference torque using speed and maximum available torque results in the generation of different speeds, which are categorized into five zones as defined in:

$$\begin{cases}\omega_r\le\omega_b\Rightarrow\text{Zone I}\\ \omega_b<\omega_r\le\omega_{end_{\mathrm{MTPA}}},T_{em}^*<T_{em_{\max\mathrm{MTPA}}}^*\Rightarrow\text{Zone II}\\ \omega_b<\omega_r\le\omega_{end_{\mathrm{MTPA}}},T_{em}^*>T_{em_{\max\mathrm{MTPA}}}^*\Rightarrow\text{Zone III}\\ \omega_{end_{\mathrm{MTPA}}}<\omega_r\le\omega_{\mathrm{inter}}\Rightarrow\text{Zone IV}\\ \omega_{\mathrm{inter}}<\omega_r\le\omega_{end_{VCLMT}},T_{em}^*<T_{em_{\max\mathrm{VCLMT}}}^*\Rightarrow\text{Zone V}\\ \text{other } T_{em_{\max\mathrm{CPR}}}^*\end{cases}.\tag{21}$$

3.1 Equations of Zone I and Zone II

At the intersection of the constant torque hyperbol (at a specific torque T_{em}^*) and the MTPA curve lies the operating

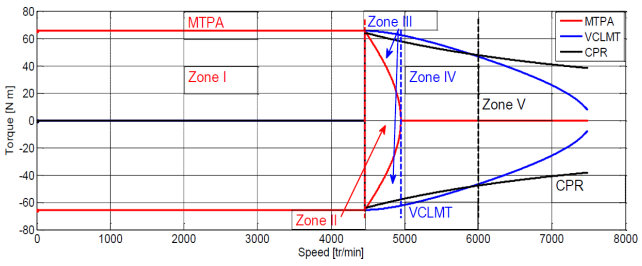

Fig. 6 Torque/speed characteristics of the proposed IPMSM

point for these zones. By solving the two-equation system, the currents values $\left(i_{dref}, i_{qref}\right)$ can be determined [24].

$$\begin{cases} i_{dref} = -\dfrac{\Phi_f}{4\left(L_d - L_q\right)} + \sqrt{\dfrac{\Phi_f^2}{16\left(L_d - L_q\right)^2} + \dfrac{i_{dref}^2 + i_{qref}^2}{2}} \\ i_{qref} = \dfrac{T_{em}^*}{\dfrac{3}{2} p\left(\Phi_f + \left(L_d - L_q\right)\right) i_{dref}} \end{cases} \tag{22}$$

As a result, we arrive at the subsequent quadratic equation.

$$i_d^4 + 3\frac{\Phi_f}{L_d - L_q} i_d^3 + 3\left(\frac{\Phi_f}{L_d - L_q}\right)^2 i_d^2 + \left(\frac{\Phi_f}{L_d - L_q}\right)^3 i_d - \left(\frac{2}{3}\frac{T_{em}^*}{p}\frac{1}{L_d - L_q}\right)^2 = 0 \tag{23}$$

Among the available solutions, the one with the most negative value is considered to be the expected useful solution.

3.2 Equations of Zone III, Zone IV and Zone V

At the point of operation within these zones, the voltage ellipse associated with a specific speed ω_r^* intersects with the constant torque hyperbol, which corresponds to a given torque T_{em}^*. By solving the system of two equations, the current values $\left(i_{dref}, i_{qref}\right)$ can be determined [24].

$$\begin{cases} \left(\Phi_f + L_d i_{dref}\right)^2 + \left(L_q i_{qref}\right)^2 = \left(\dfrac{V_{sn}}{p\omega_r^2}\right)^2 \\ i_{qref} = \dfrac{T_{em}^*}{\dfrac{3}{2} p\left(\Phi_f + \left(L_d - L_q\right) i_{dref}\right)} \end{cases} \tag{24}$$

As a result of this, we can derive the following quadratic equation.

$$\begin{aligned} & L_d^2\left(L_d - L_q\right)^2 i_d^4 + 2L_d\left(L_d - L_q\right)\left(2L_d - L_q\right)\Phi_f i_d^3 \\ & + \left(6L_d^2 - 6L_d L_q + L_q^2\right)\Phi_f^2 i_d^2 + 2\left(2L_d - L_q\right)\Phi_f^3 i_d + \Phi_f^4 \\ & + \left(\frac{2}{3}\frac{T_{em}^*}{p} L_q\right)^2 - \left(\frac{V_{sn}}{p\omega_r^*}\right)^2 \Phi_f^2 = 0 \end{aligned} \tag{25}$$

Out of all the potential solutions, the most negative one is considered to be the expected useful solution.

To determine the torque curve that distinguishes Zone II from Zone III, we can find the point where the Maximum Torque Per Ampere (MTPA) intersects with a point on the tension ellipse at reference speed ω_r^* [24].

The torque can be represented by the Eq. (26):

$$T_{em_{\max MTPA}}^* = \frac{3}{2} p\left(\Phi_f + \left(L_d - L_q\right) i_{dt}\right) i_{qt}. \tag{26}$$

The intersection of the voltage ellipse and the maximum current circle yields the current values $\left(i_{d_{VCLMT}}, i_{q_{VCLMT}}\right)$ when given a reference torque $T_{em_{\max VCLMT}}^*$ and actual speed ω_r^* [24]. The Eq. (27) represents Zone V on the curve is as follows:

$$T_{em_{\max VCLMT}}^* = \frac{3}{2} p\left(\Phi_f + \left(L_d - L_q\right) i_{d_{VCLMT}}\right) i_{q_{VCLMT}}. \tag{27}$$

The proposed combined control scheme for the motorization of an interior permanent magnet synchronous motor (IPMSM) is illustrated in Fig. 7. This scheme enables control over a wide range of operating speeds. The motor is powered by a battery and connected to a three-phase voltage source inverter. Control is implemented in the park *d–q* reference frame. The control scheme consists of four main controllers, namely: MTPA control, VCLMT control, CPR control, and vector control [25]. Each of these controllers will be discussed in detail.

4 Simulation and discussion

The simulation results achieved using the newly developed combined control strategy will be discussed in Section 4. To conduct the simulations, mathematical models of the IPMSM and various control techniques such as MTPA, VCLM, CPR, and CV were implemented on the MATLAB/Simulink software [26]. Specifically, the combined control strategy was tested for high-speed references, and a simulation test was performed accordingly.

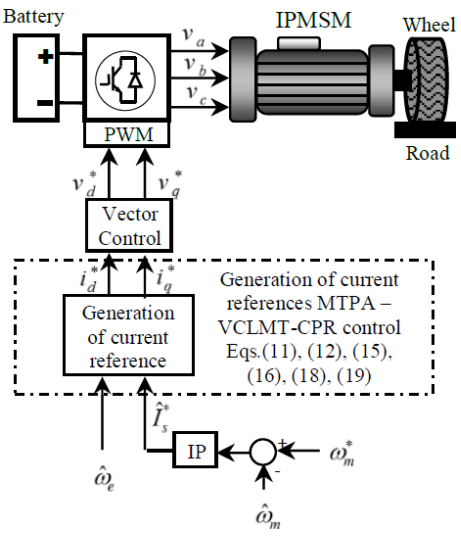

Fig. 7 Scheme of combined MTPA-VCLMT-CPR control of IPMSM

The IPMSM parameters utilized in the traction chain of an electric vehicle, along with the corresponding characteristic speeds, can be found in Table 1.

In order to assess the effectiveness of the suggested strategy across a wide range of operating speeds, we will focus on a specific operating point during traction mode, which corresponds to a reference speed of 700 rad/s.

Fig. 8 displays the speed response of the system, revealing that the initial speed of the IPMSM is rapid. Within a mere 0.14 sec, the speed stabilizes without any overshoot, enabling accurate tracking of the reference speed. Even when there is a change in load, the speed quickly adjusts and tracks the reference value, as depicted in the zoomed-in view in Fig. 8.

For the first point, at a speed below the base speed, the requested torque is higher than the maximum torque that MTPA control could deliver. At a speed between ω_b and $\omega_{end_{\mathrm{MTPA}}}$, depending on the requested torque, we could be in Zone II, Zone III, or simply governed by the torque defined by the VCLMT control strategy. For a speed between $\omega_{end_{\mathrm{MTPA}}}$ and ω_{inter}, the current references are generated by the VCLMT control strategy.

The torque response is nearly instantaneous, as shown in Fig. 9. It is important to note that the developed torque is limited to the maximum torque provided by the MTPA control in the torque region where the motor speed is below the base speed.

Furthermore, the currents reach their maximum values dictated by the MTPA control, as seen in Fig. 10 (c) and (d). Subsequently, they rapidly decrease towards the load-imposed value with minimal ripple in steady state. The current responses are illustrated in Fig. 10 (a) to (f). When the motor speed is below the base speed, which is referred to as the constant torque region, the MTPA control precisely follows the imposed current references i_d and i_q, as depicted in Fig. 10 (c) and (d). However, beyond the base speed, the VCLMT and CPR control strategies generate the current references, as shown in Fig. 10 (c) and (d). It is important to note that the d–q axis current represents the torque produced by the IPMS motor, as illustrated in Fig. 9. Additionally, Fig. 10 (f) shows the three stator currents corresponding to the specific operation being analyzed. It is worth mentioning that there is a significant transient response observed during the transient mode. Subsequently, the currents promptly adjust to any changes in the applied load.

Based on the simulation results provided, the combined control strategy that was implemented demonstrates consistent and dependable performance in both the constant torque region at low-speed and the constant power region at high-speed. Furthermore, the simulation results align with the initial analysis conducted for the combined control strategy. The expected combined control effect is achieved and the proposed method is proved feasible.

Table 1 IPMSM parameters used in EV application [24]

Symbol	Parameter	Value
Pe	Nominal power	30 kW
$\hat{T}_e$	Maximal torque	65.55 N m
V_s	Line to line voltage	230 V
R_s	Stator resistance	0.45
L_d	d-axis inductance	0.54 mH
L_q	q-axis inductance	1.05 mH
Φ_f	Permanent magnet flux linkage	0.148 Wb
p	Number of pole pairs	3
f	Friction coefficient	2.76 e^{-5}
J	Inertia coefficient	0.02 kg m^2
$\hat{I}_s$	Nominal current	100 A
ω_{base}	Based speed	466.81 rad/s
$\omega_{end_{\mathrm{MTPA}}}$	MTPA limited speed	518.02 rad/s
ω_{inter}	Intersection VCLMT-CPR speed	617 rad/s
$\omega_{end_{\mathrm{VCLMT}}}$	VCLMT limited speed	788.4 rad/s

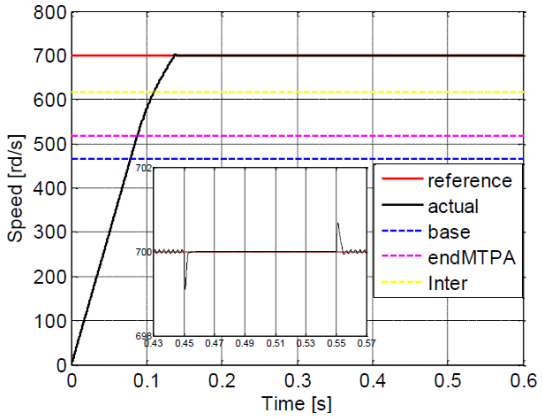

Fig. 8 Rotational speed

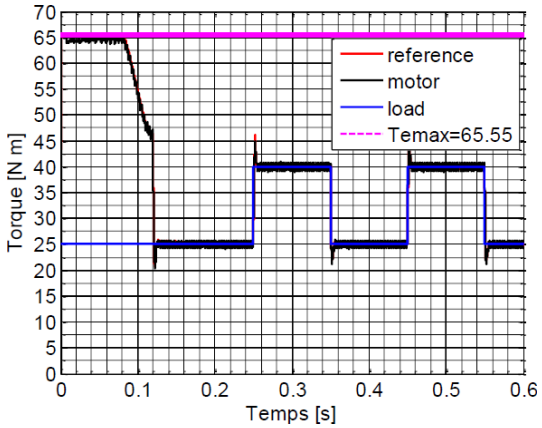

Fig. 9 Electromagnetic torque

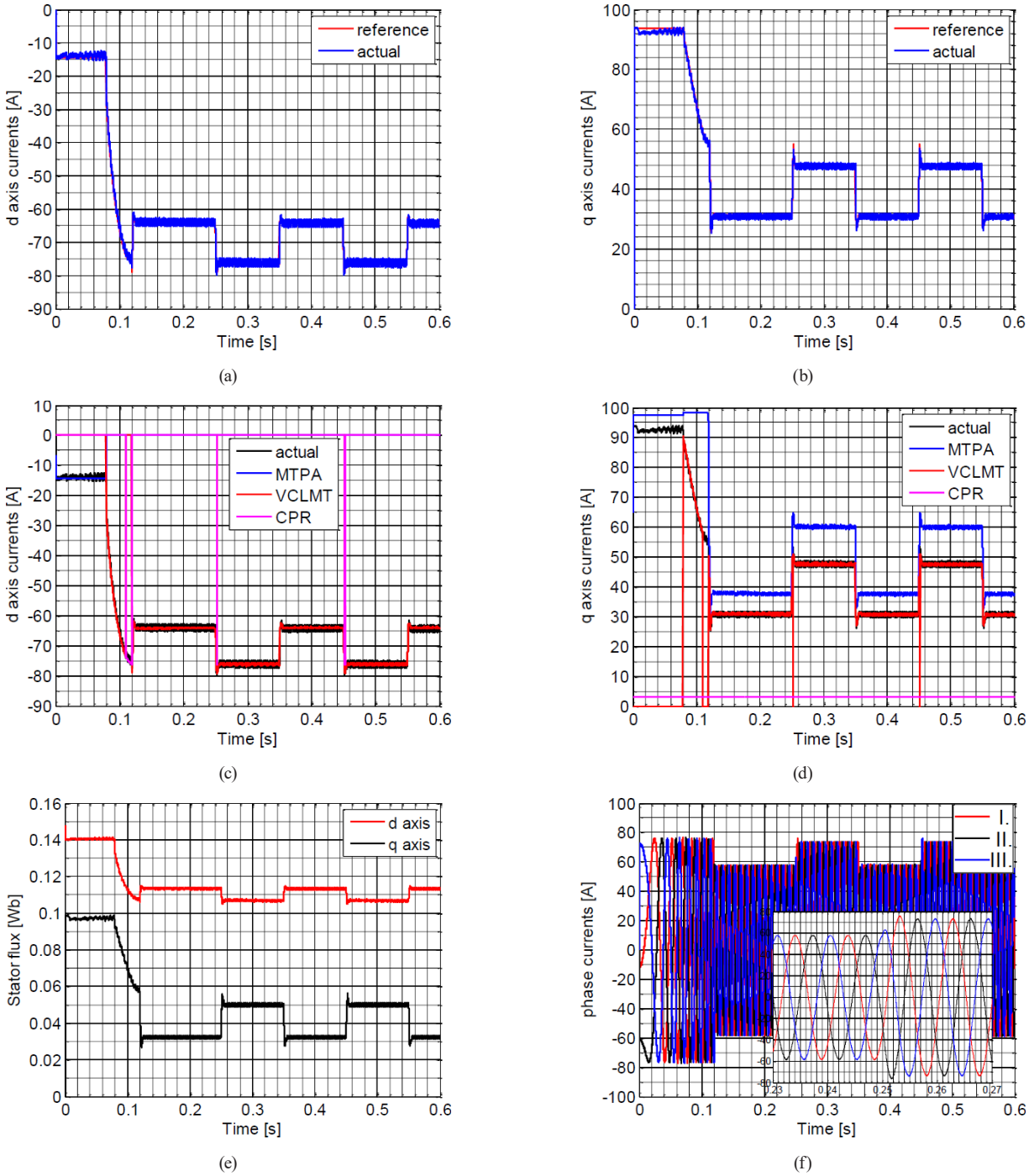

Fig. 10 Motor currents: (a) ***d***-axis currents; (b) ***q***-axis currents; (c) ***d***-axis currents MTPA, VCLMT and CPR; (d) ***q***-axis currents MTPA, VCLMT and CPR; (e) Stator flux; (f) Phase currents I., II. and III.

5 Conclusion

A novel control strategy for IPMSMs, combining three control techniques and five torque–speed operating regions, has been developed. It achieves maximum torque over a wide speed range while delivering the precise torque required by the braking system, demonstrating improved performance and efficiency in IPMSM motors drive used in electric traction applications.

The proposed method integrates three complementary control techniques: Maximum Torque Per Ampere (MTPA) control for low-speed operation, Voltage Current Limited Maximum Torque (VCLMT) control for high-speed regions, and Constant Power Region (CPR) control, also applicable at high speeds. These algorithms have been specifically formulated for IPMSMs supplied by a three-phase two-level voltage inverter. A theoretical

analysis has been conducted to evaluate the steady-state performance across the full operating speed range. Based on this analysis, a unified control scheme has been implemented, utilizing MTPA below the base speed and switching to VCLMT-CPR control above it. The effectiveness of the combined strategy was verified through numerical simulations in MATLAB/Simulink [26], demonstrating improved dynamic response and consistent performance across varying speeds. Numerical simulations confirm the stability and robustness of the proposed IPMSM control strategy. During transient conditions, the motor quickly reaches the desired torque without overshoot or oscillations, while steady-state operation maintains consistent torque and speed. These results are consistent across both low and high speed ranges, demonstrating reliable performance and effective torque regulation under varying operating conditions.

These findings not only confirm the viability of the proposed approach but also open avenues for further investigation into real-time control implementation, experimental validation on hardware platforms, and adaptation to multi-inverter or multi-motor electric drive systems.

References

[1] Sekour, M., Hartani, K., Merah, A. "Electric Vehicle Longitudinal Stability Control Based on a New Multimachine Nonlinear Model Predictive Direct Torque Control", Journal of Advanced Transportation, 2017(1), 4125384, 2017. https://doi.org/10.1155/2017/4125384

[2] Ma, C., Xu, M., Wang, H. "Dynamic emulation of road/tyre longitudinal interaction for developing electric vehicle control systems", Vehicle System Dynamics, 49(3), pp. 433–447, 2011. https://doi.org/10.1080/00423110903545172

[3] Hori, Y. "Future vehicle driven by electricity and Control-research on four-wheel-motored "UOT electric march II"", IEEE Transactions on Industrial Electronics, 51(5), pp. 954–962, 2004. https://doi.org/10.1109/TIE.2004.834944

[4] Aouadj, N., Hartani, K., Fatiha, M. "New Integrated Vehicle Dynamics Control System Based on the Coordination of Active Front Steering, Direct Yaw Control, and Electric Differential for Improvements in Vehicle Handling and Stability", SAE International Journal of Vehicle Dynamics, Stability, and NVH, 4(2), pp. 119–133, 2020. https://doi.org/10.4271/10-04-02-0009

[5] Sepulchre, L., Fadel, M., Pietrzak-David, M., Porte, G. "MTPV Flux-Weakening Strategy for PMSM High Speed Drive", IEEE Transactions on Industry Applications, 54(6), pp. 6081–6089, 2018. https://doi.org/10.1109/TIA.2018.2856841

[6] Hartani, K., Merah, A., Draou, A. "Stability Enhancement of Four-in-Wheel Motor-Driven Electric Vehicles Using an Electric Differential System", Journal of Power Electronics, 15(5), pp. 1244–1255, 2015. https://doi.org/10.6113/JPE.2015.15.5.1244

[7] Rahman, M. A., Masrur, M. A., Uddin, M. N. "Impacts of interior permanent magnet machine technology for electric vehicles", In: 2012 IEEE International Electric Vehicle Conference, Greenville, SC, USA, 2012, pp. 1–5. ISBN 978-1-4673-1561-6 https://doi.org/10.1109/IEVC.2012.6183226

[8] Itani, K., De Bernardinis, A., Khatir, Z., Jammal, A., Oueidat, M. "Regenerative Braking Modeling, Control, and Simulation of a Hybrid Energy Storage System for an Electric Vehicle in Extreme Conditions", IEEE Transactions on Transportation Electrification, 2(4), pp. 465–479, 2016. https://doi.org/10.1109/TTE.2016.2608763

[9] Itani, K., De Bernardinis, A., Khatir, Z., Jammal, A. "Optimal traction and regenerative braking reference current synthesis for an IPMSM motor using three combined torque control methods for an Electric Vehicle", In: 2016 IEEE Transportation Electrification Conference and Expo (ITEC), Dearborn, MI, USA, 2016, pp. 1–6. ISBN 978-1-5090-0403-4 https://doi.org/10.1109/ITEC.2016.7520214

[10] Li, G.-L., Luo, D., Ye,Y., Li, R. "Flux-weakening control of permanent magnet synchronous motor used in electric Vehicles", Dianli Dianzi Jishu (Power Electronics), 44(6), pp. 88–89, 2010.

[11] Liu, C., Luo, Y. "Overview of advanced control strategies for electric machines", Chinese Journal of Electrical Engineering, 3(2), pp. 53–61, 2017. https://doi.org/10.23919/CJEE.2017.8048412

[12] Liu, T., Chen, G., Li, S. "Application of Vector Control Technology for PMSM Used in Electric Vehicles", The Open Automation and Control Systems Journal, 6, pp. 1334–1341, 2014. https://doi.org/10.2174/1874444301406011334

[13] Dey, T., Mukherjee, K., Syam, P. "Dynamic adjustments of the D-Q axes reference voltage limits during flux weakening and MTPA control of an IPMSM drive for an EV application", In: 2016 2nd International Conference on Control, Instrumentation, Energy & Communication (CIEC), Kolkata, India, 2016, pp. 324–328. ISBN 978-1-5090-0035-7 https://doi.org/10.1109/CIEC.2016.7513821

[14] Kasa, N., Katsuta, T. "A Flux Weakening Control Method for In-Wheel Motor Drives of Electric Vehicles", In: 2019 IEEE 28th International Symposium on Industrial Electronics (ISIE), Vancouver, BC, Canada, 2019, pp. 209–214. ISBN 978-1-7281-3666-0 https://doi.org/10.1109/ISIE.2019.8781188

[15] Barbini, N., Bortolozzi, M., Tessarolo, A. "Performance evaluation of a vehicle traction drive based on a Permanent Magnet synchronous motor equipped with a mechanical flux weakening device", In: 2016 Eleventh International Conference on Ecological Vehicles and Renewable Energies (EVER), Monte Carlo, Monaco, 2016, pp. 1–6. ISBN 978-1-5090-2464-3 https://doi.org/10.1109/EVER.2016.7476372

[16] Lee, K.-W., Lee, S. B. "MTPA operating point tracking control scheme for vector controlled PMSM drives", In: SPEEDAM 2010, Pisa, Italy, 2010, pp. 24–28. ISBN 978-1-4244-4986-6 https://doi.org/10.1109/SPEEDAM.2010.5544955

[17] Li, M., He, J., Demerdash, N. A. O. "A flux-weakening control approach for interior permanent magnet synchronous motors based on Z-source inverters", In: 2014 IEEE Transportation Electrification Conference and Expo (ITEC), Dearborn, MI, USA, 2014, pp. 1–6. ISBN 978-1-4799-2262-8 https://doi.org/10.1109/ITEC.2014.6861776

[18] Kim, D.-Y., Lee, J.-H., Ko, A.-Y., Won, C.-Y., Kim, Y.-R. "Braking torque control method of IPMSM for electric vehicle using 2D look-up table", In: 2013 IEEE International Symposium on Industrial Electronics, Taipei, Taiwan, 2013, pp. 1–5. ISBN 978-1-4673-5193-5 https://doi.org/10.1109/ISIE.2013.6563774

[19] Schoonhoven, G., Uddin, M. N. "MTPA- and FW-Based Robust Nonlinear Speed Control of IPMSM Drive Using Lyapunov Stability Criterion", IEEE Transactions on Industry Applications, 52(5), pp. 4365–4374, 2016. https://doi.org/10.1109/TIA.2016.2564941

[20] Park, J.-H., Lee, J.-H., Lee, J.-H., Won, C.-Y. "Current control method of IPMSM in constant power region for HEV", In: 2011 International Conference on Electrical Machines and Systems, Beijing, China, 2011, pp. 1–6. ISBN 978-1-4577-1043-8 https://doi.org/10.1109/ICEMS.2011.6073677

[21] Li, Y., Zhao, S., Zhao, Y. "Stduy on Flux Weakening Speed Regulation of Permanent Magnet Synchronous Motor for Vehicle", In: 2019 Chinese Control And Decision Conference (CCDC), Nanchang, China, 2019, pp. 4928–4932. ISBN 978-1-7281-0106-4 https://doi.org/10.1109/CCDC.2019.8833220

[22] Direm, C., Hartani, K., Aouadj, N. "New Combined Maximum Torque per Ampere-Flux Weakening Control Strategy for Vehicle Propulsion System", SAE International Journal of Vehicle Dynamics, Stability, and NVH, 5(2), pp. 131–145, 2021. https://doi.org/10.4271/10-05-02-0009

[23] Aouadj, N., Hartani, K., Merah, A. "Artificial Intelligence DTC MTPA Strategy Based on Speed MRAS Observer for Electric Vehicle Traction Applications", Periodica Polytechnica Electrical Engineering and Computer Science, 69(4), pp. 386–400, 2025. https://doi.org/10.3311/PPee.41104

[24] Itani, M. K. "Energy recovery for integrated wheel-motor, electric vehicle application", PhD Thesis, Université Paris-Saclay, 2017. [online] Available at: https://theses.hal.science/tel-01558984v1 [Accessed: 10 July 2017]

[25] Novotny, D. W., Lipo, T. A. "Vector Control and Dynamics of AC Drives", Oxford University Press, 1996. ISBN 9780198564393 https://doi.org/10.1093/oso/9780198564393.001.0001

[26] The MathWorks, Inc. "MATLAB/Simulink, (R2019a)", [computer program] Available at: https://getintopc.com/softwares/development/matlab-2019-free-download-1326503/ [Accessed: 28 March 2019]